Subcycle nonadiabatic strong-field tunneling ionization

Min Li,[1,2] Ji-Wei Geng,[1] Meng Han,[1] Ming-Ming Liu,[1] Liang-You Peng,[1,3] Qihuang Gong,[1,3] and Yunquan Liu[1,3]

[1]*Department of Physics and State Key Laboratory for Mesoscopic Physics, Peking University, Beijing 100871, People's Republic of China*

[2]*School of Physics and Wuhan National Laboratory for Optoelectronics, Huazhong University of Science and Technology, Wuhan 430074, People's Republic of China*

[3]*Collaborative Innovation Center of Quantum Matter, Beijing 100871, People's Republic of China*

(Received 21 May 2014; revised manuscript received 22 November 2015; published 4 January 2016)

We present a subcycle nonadiabatic strong-field tunneling theory and derive the position of tunnel exit, the transverse and longitudinal momentum distributions at the tunnel exit, and the ionization rate in an instantaneous laser field. These tunneling coordinates are shown to nonadiabatically couple with each other in an instantaneous laser field when the electron tunnels through the barrier. We have further incorporated the nonadiabatic tunneling theory with the quantum-trajectory Monte Carlo approach to investigate the nonadiabatic effect on the photoelectron angular distributions. The simulated photoelectron angular distributions with the nonadiabatic corrections have been validated by comparison with the *ab initio* results through numerically solving the time-dependent Schrödinger equation. The nonadiabatic coordinates at the tunnel exit play important roles in both the direct ionization and rescattering process. The nonadiabatic tunneling theory provides an intuitive understanding on subcycle dynamics of tunneling ionization.

DOI: 10.1103/PhysRevA.93.013402

I. INTRODUCTION

The process of tunneling is among the most fundamental quantum processes and it is of central importance to a variety of fields. Traditionally, according to the pioneering work by Keldysh [1], the ionization rates of an atom in an alternating strong electric field in both the multiphoton and tunneling ionization can be treated with averaging over a single period of the electric field's oscillation. Perelomov *et al.* further considered arbitrary laser polarization and included the Coulomb interaction through the first-order correction in the quasiclassical action of a short-range potential (which is known as the PPT model) [2–4]. Based on the PPT theory, the Ammosov-Delone-Krainov (ADK) model is in the limit when the Keldysh parameter ($\gamma = \omega\sqrt{2I_p}/E_0$, where E_0 is the laser field amplitude, ω is the field frequency, and I_p is the ionization potential) approaches zero (quasistatic limit) [5,6]. In this adiabatic picture, the tunneling process was treated as if the electron penetrates a static or quasistatic barrier formed by the electric field and the binding potential of the atom, as the electron tunneling time is negligible compared with the period of the laser electric field.

Recently, nonadiabatic effects in the tunneling process have attracted considerable interest motivated by the precise experiments (see [7–9], for example). The reconstructed initial transverse momentum distribution at the tunnel exit in circularly polarized laser fields was shown to be larger than the prediction of the adiabatic tunneling theory [7]. As to the initial longitudinal momentum at the tunnel exit, a common assumption widely used is to set it to zero in the adiabatic picture. Through high-harmonic generation by orthogonally polarized two-color laser fields, a nonzero initial longitudinal momentum offset at the tunnel exit was revealed [8]. In a recent experiment, the width of the initial longitudinal momentum spread was claimed to be around 1 a.u. [10]. In reality, the value of the initial longitudinal momentum spread at the tunnel exit is still in debate [11,12]. By measuring the tilt angle of the photoelectron momentum distributions in an elliptically polarized laser field, it was shown that the nonadiabatic theories contradict the experimental trends of the data [9]. Subsequently, this conclusion was found to be in contrast with the findings from the *ab initio* calculations with solving the time-dependent Schrödinger equation (TDSE) [13] and the nonadiabatic simulations [14]. The most important issue we address is that, in these experimental tests of nonadiabaticity, only one physical quantity was measured and the other physical quantities were still treated in the adiabatic picture, which will lead to contradictory conclusions. We therefore believe that it is very necessary to look at subcycle ionization dynamics, including the instantaneous ionization rate [15–18] and the tunneling coordinates, in self-consistent consideration of the nonadiabatic effect for strong-field tunneling ionization.

In Sec. II of this paper, we present a subcycle nonadiabatic tunneling ionization theory based on the strong-field approximation. We obtain the nonadiabatic description of the position of the tunnel exit, the initial momentum distribution at the tunnel exit, and the ionization rate in the instantaneous laser field. All the physical quantities at the tunnel exit are strongly coupled in the laser field because of nonadiabatic effects. Especially, the distribution of the longitudinal momentum and the position of the tunnel exit are derived self-consistently. In Sec. III, we have further incorporated the nonadiabatic theory into the quantum-trajectory Monte Carlo simulation [19] to calculate the photoelectron angular distributions. We compare the calculated photoelectron angular distributions using the nonadiabatic theory with the *ab initio* results by numerically solving the TDSE. Then we conclude the topic presented in this paper.

II. NONADIABATIC MODEL

Within the strong-field approximation, the transition amplitude can be approximated by a sum over the quantum orbits using the saddle-point method (see, e.g., [20,21]),

$$M_{\mathbf{p}}^{\mathrm{SFA}} = \sum_s \frac{2^{-1/2}(2I_p)^{5/4}}{\mathbf{E}(t_s)\cdot[\mathbf{p}+\mathbf{A}(t_s)]} e^{iS_{s,\mathbf{p}}}, \tag{1}$$

where $S_{s,\mathbf{p}} = -\int dt\{\frac{1}{2}[\mathbf{p}+\mathbf{A}(ts)]^2 + I\}_p$ is the classical action and t_s is the saddle point that should satisfy

$$\frac{\partial S_{s,\mathbf{p}}}{\partial t} = \frac{1}{2}[\mathbf{p}+\mathbf{A}(t_s)]^2 + I_p = 0. \tag{2}$$

Since $I_p > 0$ and $\mathbf{p}$ is a real value, the complex time t_s can be given with $t_s = t_r + it_i$, where t_r is the ionization time and t_i is the so-called tunneling time (or Keldysh time) [1]. For a linearly polarized monochromatic laser field with $\mathbf{E}(t) = E_0\cos(\omega t)\mathbf{z}$ [the vector potential is $\mathbf{A}(t) = -\frac{E_0}{\omega}\sin(\omega t)\mathbf{z}$], the real and imaginary parts of Eq. (2) read $(p_z - E_0/\omega\sin\omega t_r\cosh\omega t_i)^2 - (E_0/\omega\cos\omega t_r\sinh\omega t_i)^2 + {p_\perp}^2 + 2I_p = 0$ and $p_z - E_0/\omega\sin\omega t_r\cosh\omega t_i = 0$, respectively.

The conserved canonical momentum $\mathbf{p} = (p_z, p_\perp)$ can be related to the momentum at the tunnel exit where the time becomes real,

$$\begin{aligned} p_z &= v_z + E_0\sin(\omega t_r)/\omega \\ p_\perp &= v_\perp, \end{aligned} \tag{3}$$

where v_z and $v_\perp$ are the initial longitudinal and transverse momentum with respect to the laser polarization direction at the tunnel exit point. Combining those relations, we can establish the relation of the ionization time (t_r) and the tunneling time (t_i) as

$$\sinh\omega t_i = \gamma(t_r, v_\perp), \tag{4}$$

and we can also obtain the nonadiabatic longitudinal momentum at the tunnel exit,

$$v_z = \frac{E_0\sin\omega t_r}{\omega}[\sqrt{1+\gamma^2(t_r,v_\perp)} - 1], \tag{5}$$

where the effective Keldysh parameter is given by $\gamma(t_r, v_\perp) = \omega\sqrt{2I_p + {v_\perp}^2}/|E(t_r)|$. Both the tunneling time and the initial longitudinal momentum are functions of the parameter $\gamma(t_r, v_\perp)$. Different with the Keldysh parameter, $\gamma(t_r, v_\perp)$ depends on the ionization time and the initial transverse momentum [22].

The instantaneous ionization rate is determined by the classical action under the barrier, given by

$$S_{s,\mathbf{p}} = -\int_{t_s}^{t_r} dt\left\{\frac{1}{2}[\mathbf{p}+\mathbf{A}(t)]^2 + I_p\right\}. \tag{6}$$

Inserting the laser field into the above equation, one obtains $S_{s,\mathbf{p}} = i[\frac{p^2}{2} + I_p + U_p]t_i - p_z\frac{E_0}{\omega^2}(\cos\omega t_r - \cos\omega t_s) + \frac{{E_0}^2}{8\omega^3}(\sin 2\omega t_r - \sin 2\omega t_s)$. The real part and the imaginary part, respectively, read $\mathrm{Re}S_{s,\mathbf{p}} = -p_z\frac{E_0}{\omega^2}\cos\omega t_r(1-\cosh\omega t_i) + \frac{{E_0}^2}{8\omega^3}\sin 2\omega t_r(1-\cosh 2\omega t_i)$ and $\mathrm{Im}S_{s,\mathbf{p}} = (\frac{p^2}{2} + I_p + U_p)t_i - p_z\frac{E_0}{\omega^2}\sin\omega t_r\sinh\omega t_i - \frac{{E_0}^2}{8\omega^3}\cos 2\omega t_r\sinh 2\omega t_i$, where $U_p = \frac{E_0^2}{4\omega^2}$ is the ponderomotive energy. The real part of the subbarrier action is related to a phase shift for the trajectory under the barrier [21], and the imaginary part is related to the ionization rate.

We further consider the preexponential factor in Eq. (1); we set $R = \mathbf{E}(t_s)\cdot[\mathbf{p}+\mathbf{A}(t_s)]$, whose real and imaginary parts are given by $R_1 = -\gamma^2(t_r,v_\perp)\frac{{E_0}^2}{\omega}\sin\omega t_r\cos\omega t_r$ and $R_2 = -\frac{{E_0}^2\cos^2\omega t_r}{\omega}\gamma(t_r,v_\perp)\sqrt{1+\gamma^2(t_r,v_\perp)}$, respectively. Thus the nonadiabatic instantaneous ionization rate can be expressed as

$$\begin{aligned} W(t_r,v_\perp) = {} & \frac{\omega^2(2I_p)^{5/2}}{2{E_0}^4\gamma^2(t_r,v_\perp)[\gamma^2(t_r,v_\perp)+\cos^2\omega t_r]\cos^2\omega t_r} \\ & \times\exp\left(-\frac{{E_0}^2}{\omega^3}\left\{\left[\sin^2\omega t_r + \gamma^2(t_r,v_\perp) + \frac{1}{2}\right]\right.\right. \\ & \times\sinh^{-1}\gamma(t_r,v_\perp) \\ & \left.\left. -\frac{1}{2}\gamma(t_r,v_\perp)\sqrt{1+\gamma^2(t_r,v_\perp)}(1+2\sin^2\omega t_r)\right\}\right). \end{aligned} \tag{7}$$

Another important tunneling coordinate is the position of the tunnel exit point. In the nonadiabatic picture, the tunnel exit is related to the sub-barrier trajectory $\mathbf{r}(t_r) = \int_{t_s}^{t_r} dt[\mathbf{p}+\mathbf{A}(t)]$. In the linearly polarized laser field, it is given by

$$z(t_r,v_\perp) = p_x(t_r - t_s) + \frac{E_0}{\omega^2}(\cos\omega t_r - \cos\omega t_s). \tag{8}$$

The tunnel exit point is the real part of Eq. (8) [23],

$$\mathrm{Re}z(t_r,v_\perp) = \frac{E_0}{\omega^2}\cos\omega t_r[1-\sqrt{1+\gamma^2(t_r,v_\perp)}]. \tag{9}$$

The subcycle tunneling coordinates have been derived. From Eqs. (4), (5), and (9), one can find that all those tunneling coordinates are coupled with each other at an instantaneous laser phase.

III. RESULTS AND DISCUSSIONS

Using the Monte Carlo method, we have calculated the nonadiabatic tunneling coordinates of H atoms in a linearly polarized laser field at the intensity of 1×10^{14} W/cm^2 (800 nm), as shown in Fig. 1. With averaging over a single laser cycle, both the longitudinal momentum and transverse momentum at the tunnel exit reveal the Gaussian distribution [Fig. 1(a)]. As shown in Fig. 1(b), the initial transverse momentum shows a time-dependent Gaussian distribution with respect to the laser phase. Usually, the longitudinal momentum at the tunnel exit was assumed to be zero in the adiabatic tunneling picture. In the nonadiabatic picture, one can see that the longitudinal momentum at the tunnel exit depends on the ionization phase with respect to the laser field (or the vector potential) [Fig. 1(c)]. Since most of electrons tunnel near the field maximum where the vector potential is zero, the longitudinal momentum assumed to be zero is a good approximation in the adiabatic limit. However, the parameter $\gamma(t_r, v_\perp)$ will increase when the electrons tunnel at a laser phase away from the field maximum. Thus, the initial longitudinal momentum at the tunnel exit and nonadiabatic effects become largely important when the vector potential increases [8].

In the nonadiabatic picture, the tunnel exit is not fixed with respect to the instantaneous laser field, and the tunnel barrier is nonadiabatically mediated by the oscillating field. The tunnel exit depends on the instantaneous laser field and the initial transverse momentum. Compared with the adiabatic tunnel exit [the white solid line in Fig. 1(d)], the position of the nonadiabatic tunnel exit exhibits a broader distribution and is closer to the nucleus, as seen in Fig. 1(d).

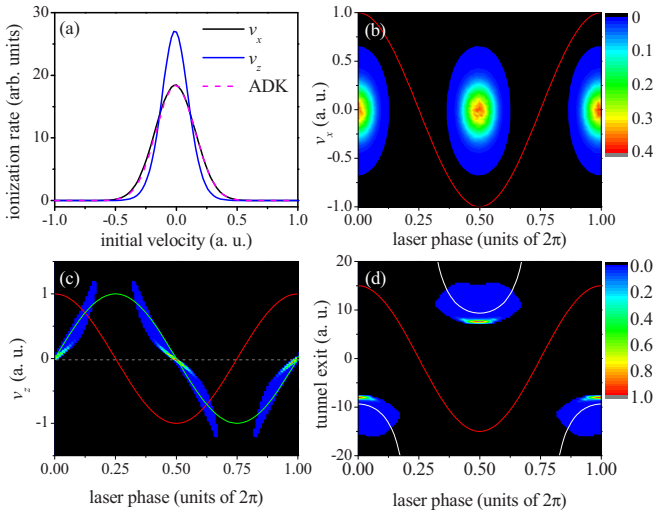

FIG. 1. The nonadiabatic tunneling coordinates. (a) The cycle-averaged longitudinal momentum distribution and transverse momentum distributions at the tunnel exit. The dashed curve shows the cycle-averaged transverse momentum distribution predicted by ADK theory. (b,c) show the transverse momentum and the longitudinal momentum distribution at the tunnel exit with respect to the tunneling phase, respectively. (d) The distribution of the tunnel exit with respect to the tunneling phase. The white curves in (d) show the tunnel exit $z_e = -I_p/E(t_r)$ in the adiabatic picture. The light field [the red solid curve in (b–d)] and the negative value of the vector potential [the green solid curve in (c)] are shown in arbitrary units.

We show the calculated width of the cycle-averaged transverse and longitudinal momentum distribution at the tunnel exit with respect to the laser intensity (800 and 1400 nm) in Fig. 2 by the Gaussian fit. The width of the transverse momentum distribution increases with the laser intensity. Instead, the width of the longitudinal momentum distribution decreases with the laser intensity, i.e., the nonadiabatic tunneling correction can converge to the adiabatic theory when the Keldysh parameter approaches zero. Increasing the laser wavelength to 1400 nm, the cycle-averaged width of the

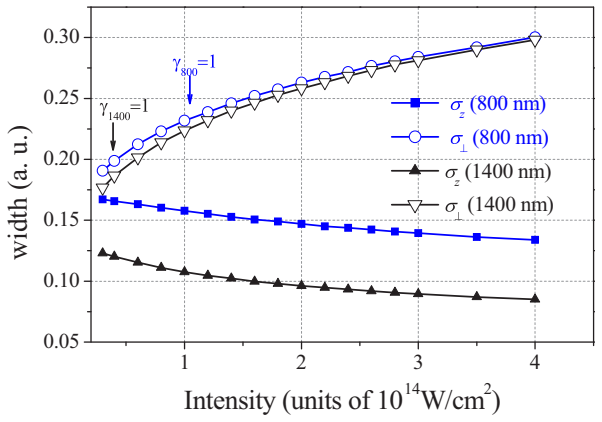

FIG. 2. The width of the cycle-averaged longitudinal momentum distribution and transverse momentum distributions at the tunnel exit with respect to the laser intensity at 800 and 1400 nm, respectively.

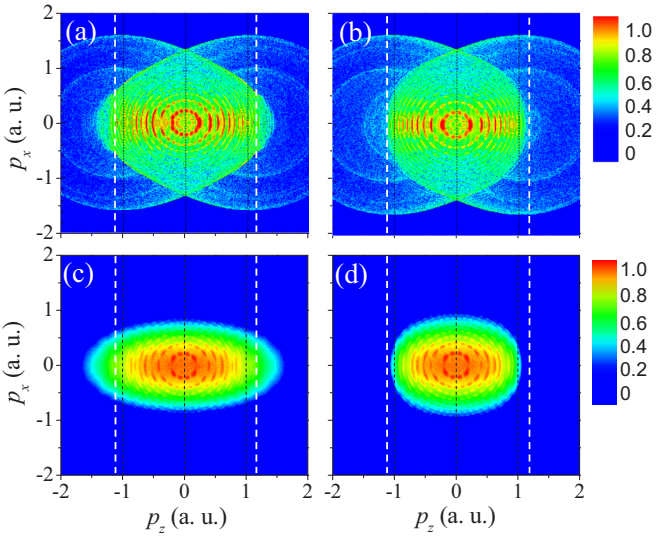

FIG. 3. The simulated photoelectron angular distributions of H atoms using the nonadiabatic (a,c) and adiabatic (b,d) tunneling theory at the intensity of 1.5×10^{14} W/cm^2 (800 nm). In order to remove the rescattering effect, the Coulomb potential effect is not included in the electron propagation after the tunneling in (c,d). The white dashed lines show the position of $\pm E_0/\omega$.

longitudinal momentum distribution substantially decreases, while the width of the transverse momentum distribution is slightly changed. Thus, it will be difficult to reveal the nonadiabatic tunneling effect by measuring the wavelength-dependent transverse momentum distributions [7].

We further investigate the nonadiabatic effect on the photoelectron angular distributions, which can be directly compared with the *ab initio* TDSE calculation. We incorporate the nonadiabatic tunneling coordinates into the quantum-trajectory Monte Carlo approach [19]. Briefly, the subsequent electron motion after the tunneling is calculated with the combination of the Newtonian equation [$\ddot{\mathbf{r}} = -Z\mathbf{r}/r^3 - \mathbf{E}(t)$] and the phase equation [$S = \int_{t_0}^{\infty} (\mathbf{v}(t)^2/2 - Z/|\mathbf{r}(t)| + I_p)dt$] in the presence of the combined Coulomb and laser fields, where r is the distance between electron and nucleus and Z is the nuclear charge. The trajectories will interfere with each other when their asymptotic momenta are the same. In all the calculations, we use a nine-cycle laser pulse (two-cycle ramp-on, five-cycle constant amplitude, and two-cycle ramp-off). The simulated photoelectron electron angular distributions for H atoms at 800 nm at 1.5×10^{14} W/cm^2 using the nonadiabatic theory are shown in Figs. 3(a) and 3(c) with ($Z = 1$) and without ($Z = 0$) considering the Coulomb potential and the rescattering effect, respectively.

For comparison, we have also performed the adiabatic calculations using the adiabatic tunneling coordinates according to the ADK model [5,6]. The position of tunnel exit is calculated with the Landau-Lifshitz theory [24], which is given by $z_e \approx -I_p/E(t_r)$ [the white solid curve in Fig. 1(d)]. The cycle-averaged transverse momentum distribution predicted by the ADK theory for H atom at 1×10^{14} W/cm^2 is comparable with the nonadiabatic transverse momentum, as seen in the dashed curve in Fig. 1(a). In the adiabatic model, we take the longitudinal momentum along the laser polarization direction

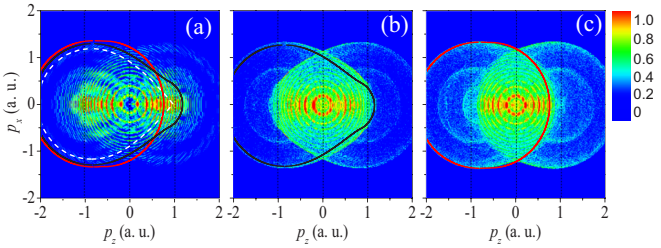

FIG. 4. The calculated two-dimensional photoelectron angular distributions of H atom with the TDSE (a), nonadiabatic tunneling theory (b), and adiabatic tunneling theory (c) at the intensity of 1×10^{14} W/cm^2 (800 nm). The black solid, red solid, and white dashed curves show the momentum cutoff predicted by the nonadiabatic theory, the adiabatic theory, and the simple model with zero initial position and momentum, respectively.

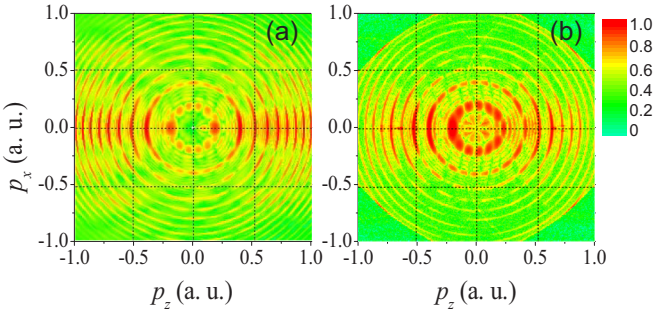

FIG. 5. The low-energy photoelectron angular distributions using the TDSE (a) and the nonadiabatic theory (b) at the intensity of 1×10^{14} W/cm^2 (800 nm).

as zero. The simulated photoelectron angular distributions for H atoms at 1.5×10^{14} W/cm^2 (800 nm) with the adiabatic tunneling theory are shown in Figs. 3(b) and 3(d) with ($Z = 1$) and without ($Z = 0$) considering the Coulomb potential and the rescattering effect, respectively.

The overall structure of the simulated photoelectron angular distributions based on the nonadiabatic and adiabatic models look quite similar. With the inclusion of the Coulomb potential, the multiple rescattering rings [25] can be recaptured by both nonadiabatic and adiabatic models. However, there are important differences caused by the nonadiabatic effects, as will be discussed below.

In order to validate the nonadiabatic theory, we now compare photoelectron angular distributions with the *ab initio* TDSE calculation. In Fig. 4(a) we present the calculated photoelectron angular distributions of the ionization of H atom by TDSE in a linearly polarized laser field at 1×10^{14} W/cm^2 (800 nm). The final photoelectron angular distributions are obtained by projecting the wave function onto the Coulomb continuum scattering eigenstates after the time-dependent propagation using a grid-based split-operator method [26]. In Figs. 4(b) and 4(c) we also present the results of the nonadiabatic and adiabatic tunneling theory at the same laser parameters, respectively.

As discussed above, in the nonadiabatic picture, the tunneling coordinates are very important, and will have significant effects on both the direct ionization electrons and rescattered electrons. We will extract the nonadiabatic effect on photoelectron angular distributions by the comparison with the *ab initio* TDSE calculation in which all effects are naturally included.

We first look at the low-energy photoelectron angular distribution, which is mostly related to the direct ionization electrons. In the adiabatic picture, with the longitudinal momentum at the tunnel exit taken as zero, the direct ionization electrons can usually obtain an energy below $2U_p$ ($|p_z| < E_0/\omega$), as seen in the white lines in Fig. 3. However, in the nonadiabatic picture, because of the initial longitudinal momentum at the tunnel exit, some direct ionization electrons can obtain a final energy larger than $2U_p$. We also show the comparison of the low-energy photoelectron angular distributions between the results using the TDSE and the nonadiabatic theory in Fig. 5.

One can find that the detailed interference structure of low-energy photoelectrons calculated by the nonadiabatic theory [Fig. 5(b)] agrees with the TDSE result [Fig. 5(a)]. In order to reveal the nonadiabatic effect on the low-energy electrons more clearly, we have removed the Coulomb potential effect and the rescattering effect after the tunneling. As seen in Figs. 3(c) and 3(d), the longitudinal momentum spreads much broader than the adiabatic case. It should be noted that the TDSE result reveals a minimum when $p_z = 0$ while the nonadiabatic simulation reveals a maximum for the first-order above threshold ionization (ATI) ring. This difference comes from the negligence of the sub-barrier Coulomb-corrected phase [21] in the nonadiabatic simulation.

As to the rescattered electrons, one can compare the cutoff in the momentum distribution of the TDSE result with that of the nonadiabatic or the adiabatic theory. The cutoff on photoelectron angular distributions can be obtained using the rescattering model [27–29]. The electron velocity before recollision can be calculated as $v_z(t) = v_{z0} - E_0/\omega[\sin(\omega t) - \sin(\omega t_0)]$, where v_{z0} is the initial longitudinal momentum given by Eq. (5) in the nonadiabatic picture and it is zero in the adiabatic picture. For these re8scattered electrons, the recollision time t_c can be obtained by numerically solving the classical equation of motion $E_0/\omega^2[\cos(\omega t_c) - \cos(\omega t_0) + \omega(t_c - t_0)\sin(\omega t_0)] + v_{z0}(t_c - t_0) + z_e = 0$, where z_e is the tunnel exit point. At t_c, the electron is elastically rescattered off the nucleus with a scattering angle with respect to its impact direction. The asymptotic momentum of the rescattered electron is $P_Z = F_0/\omega\sin(\omega t_c) + v_c\cos(\theta_c)$ and $p_x = v_c\sin(\theta_c)$, where $v_c = v_z(t_c)$ is the electron momentum at recollision. We choose the maximum and the minimum of p_z at each p_x to obtain the cutoff in the momentum plane. The calculated ring of the largest rescattering momentum cutoff is illustrated as the black and red solid lines in Figs. 4(b) and 4(c) for the nonadiabatic and adiabatic theory (with or without the initial longitudinal momentum), respectively [30]. If one takes the initial longitudinal momentum and the tunnel exit point to be zero (the initial condition of the so-called Simpleman model, which was initially proposed by van Linden van den Heuvell and Muller [31]), the calculated boundary is shown as the white dashed curve in Fig. 4(a). One can see that, considering the nonadiabatic corrections to the initial longitudinal momentum distribution and the position of tunnel exit, the calculated cutoff boundary [the black solid line in Figs. 4(a) and 4(b)] agrees

well with the results using both the TDSE calculation and the nonadiabatic quantum-trajectory Monte Carlo simulation. In this spirit, nonadiabatic corrections should be important for the phenomena closely related with the rescattering in strong-field community, e.g., high-harmonic generation and nonsequential double ionization.

IV. CONCLUSION

In summary, all the tunneling coordinates at the tunnel exit have been derived nonadiabatically in a subcycle time scale. We have shown that these tunneling coordinates are correlated in the instantaneous laser field. The nonadiabatic results will converge to the ADK theory in the adiabatic limits. We further incorporate the nonadiabatic corrections into the quantum-trajectory Monte Carlo model to calculate the photoelectron angular distributions. The photoelectron angular distributions calculated by the nonadiabatic model have been validated by the *ab initio* TDSE results. Compared with the quantum simulation, the nonadiabatic quantum-trajectory Monte Carlo approach makes the strong-field ionization more transparent and all spectral features can be interpreted in terms of trajectories. The semiclassical nonadiabatic model sketched above provides intuitive insights and possesses a predictive power for strong-field tunneling ionization.

ACKNOWLEDGMENTS

This work is supported by the National Program on Key Basic Research Project (Grant No. 2013CB922403) and the National Science Foundation of China (Grants No. 11434002 and No. 11125416).

[1] L. V. Keldysh, Sov. Phys. JETP **20**, 1307 (1965).
[2] A. M. Perelomov, V. S. Popov, and M. V. Terent'ev, Sov. Phys. JETP **23**, 924 (1966).
[3] A. M. Perelomov, V. S. Popov, and M. V. Terent'ev, Sov. Phys. JETP **24**, 207 (1967).
[4] A. M. Perelomov and V. S. Popov, Sov. Phys. JETP **25**, 336 (1967).
[5] M. V. Ammosov, N. B. Delone, and V. P. Krainov, Sov. Phys. JETP **64**, 1191 (1986).
[6] N. B. Delone and V. P. Krainov, J. Opt. Soc. Am. B **8**, 1207 (1991).
[7] L. Arissian, C. Smeenk, F. Turner, C. Trallero, A. V. Sokolov, D. M. Villeneuve, A. Staudte, and P. B. Corkum, Phys. Rev. Lett. **105**, 133002 (2010).
[8] D. Shafir, H. Soifer, B. D. Bruner, M. Dagan, Y. Mairesse, S. Patchkovskii, M. Yu. Ivanov, O. Smirnova, and N. Dudovich, Nature (London) **485**, 343 (2012).
[9] R. Boge, C. Cirelli, A. S. Landsman, S. Heuser, A. Ludwig, J. Maurer, M. Weger, L. Gallmann, and U. Keller, Phys. Rev. Lett. **111**, 103003 (2013).
[10] A. N. Pfeiffer, C. Cirelli, A. S. Landsman, M. Smolarski, D. Dimitrovski, L. B. Madsen, and U. Keller, Phys. Rev. Lett. **109**, 083002 (2012).
[11] M. Li, Y. Liu, H. Liu, Q. Ning, L. Fu, J. Liu, Y. Deng, C. Wu, L.-Y. Peng, and Q. Gong, Phys. Rev. Lett. **111**, 023006 (2013); X. Sun, M. Li, J. Yu, Y. Deng, Q. Gong, and Y. Liu, Phys. Rev. A **89**, 045402 (2014).
[12] C. Hofmann, A. S. Landsman, A. Zielinski, C. Cirelli, T. Zimmermann, A. Scrinzi, and U. Keller, Phys. Rev. A **90**, 043406 (2014).
[13] I. A. Ivanov and A. S. Kheifets, Phys. Rev. A **89**, 021402(R) (2014).
[14] M. Klaiber, K. Z. Hatsagortsyan, and C. H. Keitel, Phys. Rev. Lett. **114**, 083001 (2015).
[15] G. L. Yudin and M. Y. Ivanov, Phys. Rev. A **64**, 013409 (2001).
[16] M. Y. Ivanov, M. Spanner, and O. Smirnova, J. Mod. Opt. **52**, 165 (2005).
[17] D. I. Bondar, Phys. Rev. A **78**, 015405 (2008).
[18] L. Torlina and O. Smirnova, Phys. Rev. A **86**, 043408 (2012).
[19] M. Li, J.-W. Geng, H. Liu, Y. Deng, C. Wu, L.-Y. Peng, Q. Gong, and Y. Liu, Phys. Rev. Lett. **112**, 113002 (2014); M. Li, J.-W. Geng, M.-M. Liu, X. Zheng, L.-Y. Peng, Q. Gong, and Y. Liu, Phys. Rev. A **92**, 013416 (2015).
[20] D. B. Milošović, G. G. Paulus, D. Bauer, and W. Becker, J. Phys. B **39**, R203 (2006).
[21] T. M. Yan and D. Bauer, Phys. Rev. A **86**, 053403 (2012); T. M. Yan, S. V. Popruzhenko, M. J. J. Vrakking, and D. Bauer, Phys. Rev. Lett. **105**, 253002 (2010).
[22] $\gamma(t_r, v_\perp)$ will reduce to the Keldysh parameter for the electron released at the field maximum with zero initial transverse momentum.
[23] In the adiabatic limit $\gamma(t_r, v_\perp) \to 0$, the tunnel exit point is at the origin, which is used in Ref. [27]. Expanding Eq. (9) in a Taylor series up to the first order with respect to $\gamma(t_r, v_\perp)$, we obtain $\mathrm{Re}z(t_r) = -I_p/E(t_r)$, which is used for a short-range potential. For the electron released at the laser maximum with zero transverse momentum, Eq. (9) is the same as that in Ref. [3].
[24] L. D. Landau and E. M. Lifschitz, *Quantum Mechanics (Nonrelativistic Theory)* (Oxford University Press, New York, 1958).
[25] Y. Huismans *et al.*, Science **331**, 61 (2011).
[26] L. Peng, E. Pronin, and A. Starace, New J. Phys. **10**, 025030 (2008).
[27] P. B. Corkum, Phys. Rev. Lett. **71**, 1994 (1993).
[28] G. G. Paulus, W. Becker, W. Nicklich, and H. Walther, J. Phys. B **27**, L703 (1994).
[29] M. Li, J. Yuan, X. Sun, J. Yu, Q. Gong, and Y. Liu, Phys. Rev. A **89**, 033425 (2014).
[30] Because the tunnel exit is divergent when the laser field is close to zero, we have discarded those trajectories with very low ionization probabilities.
[31] See H. B. van Linden van den Heuvell and H. G. Muller, in *Multiphoton Processes*, edited by S. J. Smith and P. L. Knight (Cambridge University Press, Cambridge, 1988).